Geol. Mag. **156** (*7*), *2019, pp. 1175–1189* © *Cambridge University Press 2018*
doi:10.1017/S001675681800033X

Metamorphic evolution and age constraints of the garnet-bearing mica schist from the Xindaduo area of the Sumdo (U)HP metamorphic belt, Tibet

CONG ZHANG*‡†, THOMAS BADER§, LINGMIN ZHANG¶, TINGTING SHEN*, PENG LI* & XUPING LI‡

*Key Laboratory of Deep-Earth Dynamics of MLR, Institute of Geology, Chinese Academy of Geological Sciences, Beijing 100037, China
‡College of Earth Science and Engineering, Shandong University of Science and Technology, Qingdao 266590, China
§School of Earth and Space Sciences, Peking University, Beijing 100087, China
¶State Key Laboratory of Marine Geology, Tongji University, Shanghai 200092, China

(*Received* 14 September 2017; *accepted* 8 April 2018; *first published online* 15 May 2018)

Abstract – As one of the major components of the Himalayan–Tibetan Orogeny, the Lhasa terrane plays a key role in understanding the origin and evolution of this giant orogenic belt and the opening and closure of the Tethys oceans. The eclogite-bearing Sumdo Complex in the central Lhasa terrane was recognized as the main suture of the Palaeo-Tethys Ocean between the north and south Lhasa sub-terranes. Despite the eclogite having been studied for a long time, no attempts have been applied to studying the country rocks, causing confusion in understanding the relationship between the eclogite and the adjacent schist. Petrological investigations and phase equilibrium calculations on the garnet-bearing mica schist of the Sumdo Complex have been performed to constrain its metamorphic evolution. The *P–T* conditions for three metamorphic stages are constrained as P1 (480–500 °C, 2.6–2.7 GPa), P2 (580–600 °C, 1.3–1.4 GPa) and R (530 °C, 0.9 GPa), which represent the prograde, temperature peak and retrograde stages. Two possible *P–T* paths were constructed, which experienced isothermal decompression (PT1) or heating with a decompression process (PT2), corresponding to the growth and extinction of garnet porphyroblasts in the matrix. The LA-MC-ICP-MS U–Pb dating method yielded a metamorphic age of 229.7 ± 3.5 Ma, which was interpreted as the age of amphibolite-facies metamorphism at *c*. 600 °C, 1.2–1.4 GPa during the closure of the Palaeo-Tethys Ocean, resulting in the aggregation of the north and south Lhasa sub-terranes. The close relationship between the eclogite and garnet-bearing mica schist, and their similar *P–T–t* paths indicate an *in situ* tectonic evolution rather than tectonic juxtaposition during exhumation.

Keywords: garnet-bearing mica schist, garnet regrowth, metamorphic evolution, zircon ages, Sumdo Complex, Tibet

1. Introduction

Eclogites and associated (U)HP metamorphic rocks in orogenic belts record detailed *P–T* information that allows a reconstruction of the pressure and temperature paths of the subducted lithospheric crust with time (Carswell, 1990; Coleman & Wang, 1995; Ernst, 2001; Ernst & Liou, 2008). Eclogite-bearing terranes record information on the formation of tectonometamorphic belts that exhibit different types of regional metamorphic events and outline various tectonic settings (e.g. Chopin, 2003; Ernst, Hacker & Liou, 2007; Zheng, 2012). Two distinct types of convergent plate boundaries have been identified: the so-called Alpine-type and Pacific-type collisional margins (Liou *et al.* 2009). Eclogite from Alpine-type orogens is enclosed mainly in granulitic/tonalitic gneiss with minor intercalations of metapelite, as is the case for the Western Gneiss Region in SW Norway, and the Dabie-Sulu and North Qaidam orogens in China (e.g. Carswell & Cuthbert, 2003; Zhang *et al.* 2010, 2017; Song *et al.* 2014). In contrast, Pacific-type orogens represent the subduction of oceanic lithosphere, which develops a series comprising a fore-arc basin, an accretionary complex and/or a volcanic arc (Ernst & Liou, 1995; Maruyama, Liou & Terabayashi, 1996; Liou *et al.* 2004). Eclogite within Pacific-type orogens, mainly represented by structurally dismembered ophiolites, is always metamorphosed under high-pressure, low-temperature (HP–LT) conditions associated with relatively lower grade metamorphic mica schists, e.g. the Monviso massif in the Western Alps and the North Qilian and western Tianshan ultra-high-pressure (UHP) belts in western China (e.g. Chopin, 1984; Philippot & van Roermund, 1992; Zhang *et al.* 2003; Song *et al.* 2006). As the main component and usually the country rock of the eclogite in both types of orogen, metapelitic rocks record much information for understanding the evolution of subduction zones. However, owing to the various field occurrences and their simple mineral

†Author for correspondence: congzhang@pku.edu.cn

assemblages, it has for a long time been debated whether the relationship between the pelitic rocks and eclogite in a subduction zone represents '*in situ* metamorphism' or 'tectonic emplacement'. Some researchers support the *in situ* metamorphism theory on the basis of similar *P–T* trajectories and high-pressure index minerals in both the eclogite and the metapelite, like in the southwestern Tianshan, Qaidam and Dabieshan (U)HP metamorphic belts (Zheng *et al.* 2003; Zhang *et al.* 2008; Du *et al.* 2011; Zhang, C. *et al.* 2012). In contrast, other researchers insist that the eclogite and country rock were rather juxtaposed by tectonic events (Smith, 1988). As felsic rocks contain a higher proportion of hydrous phases and are rheologically weaker than their mafic counterparts, (U)HP assemblages in felsic rocks are generally prone to being modified, and peak metamorphic mineral assemblages may not be preserved (e.g. Proyer, 2003; Menold *et al.* 2009). For this reason, it is difficult to constrain the relationship only by utilizing the preservation of (U)HP assemblages. More in-depth investigations, such as detailed mineralogy and accessory mineral geochronology, need to be performed in order to illustrate the metamorphic evolution, which may yield more specific behaviours of both the eclogite and metapelite in the subduction zone.

The Lhasa terrane in SW Tibet represent one of the major core components of the Himalayan–Tibetan orogeny (Fig. 1a, b), the Earth's youngest and probably also most spectacular orogenic belt that formed by continent–continent collision after closure of the intermediate Tethys Ocean that was located in between Laurasia (Qiangtang, Songpan–Ganze and Kunlun terranes) and Gondwana (Fig. 1b). Previous ideas divided the Lhasa terrane into northern, central and southern sub-terranes, separated by the Shiquanhe–Nam Tso Mélange and the Luobadui–Milashan Fault, respectively (Pan *et al.* 2006; Zhu *et al.* 2011*b*). The dichotomy of the Lhasa terrane has been accepted since the discovery of UHP eclogite in the Sumdo Complex (Yang *et al.* 2006, 2009). Geochemical and isotopic data show that the eclogites were derived from either a mid-ocean ridge basalt (MORB) or an oceanic island basalt (OIB) protolith and experienced eclogite-facies metamorphism during Late Permian to Early Triassic times (Yang *et al.* 2009; Cheng *et al.* 2012, 2015; Cao *et al.* 2017; Zhang *et al.* 2018). *P–T* conditions of the eclogite from the Sumdo Complex have been reported by several researchers, ranging from 450–800 °C and 2.5–3.9 GPa (Yang *et al.* 2009, 2014; Zhang, Zhang & Zhao, 2011; Cheng *et al.* 2012, 2015; Zhang *et al.* 2018). These *P–T* conditions are located within the lawsonite eclogite (LE), epidote eclogite (EE) or the dry eclogite stability fields formed by low-temperature (LT) to medium-temperature (MT) metamorphism. Despite the close relationship between the eclogite and the metapelitic rocks, little attention has been paid to the eclogite country rocks such as white mica- or biotite-bearing schist. Yang *et al.* (2005) proposed that the Sumdo Complex formed at 0.93–1.15 GPa and 500–553 °C, calculated by conventional garnet–biotite and garnet–hornblende geothermobarometry on biotite schist from the nearby Mozhugongka area. Li *et al.* (2009) considered that the ductile shear processes in the Sumdo Complex occurred at 220–230 Ma, on the basis of ^{40}Ar–^{39}Ar muscovite isotopic dating. However, no attempt has been made to address the metamorphic processes and *P–T* conditions of the garnet-bearing mica schist in the Sumdo Complex, maybe because of the simple mineral assemblage, making it difficult to obtain the metamorphic conditions by conventional geothermobarometry (Le Goff & Bellevre, 1990; Proyer, 2003; Wei *et al.* 2009; Wei, 2012).

In this contribution, detailed mineralogical investigations have been applied to the garnet-bearing mica schist in the Xindaduo area (Fig. 1c) with the help of phase equilibrium calculations using Domino/Theriak software, which constrained a HP–LT eclogite-facies metamorphism followed by either heating decompression or an isothermal decompression process during retrogression. By means of the laser ablation multi-collector inductively coupled plasma mass spectrometry (LA-MC-ICP-MS) zircon U–Pb dating method, a Middle Triassic metamorphic age was also obtained from the same sample, which further restricted the relationship between the eclogite and the mica schist.

2. Geological setting

The Himalayan–Tibetan orogenic belt is classically considered to be composed of four continental terranes, called the Songpan–Ganzi, Qiangtang, Lhasa and Tethyan–Himalayan terranes from north to south (Fig. 1a, b), which are separated by the Jinsha suture zone (JSSZ), the Bangong–Nujiang suture zone (BNSZ) and the Yarlung Zangbo suture zone (YZSZ), interpreted to represent major structural elements of the Palaeo-, Meso- and Neo-Tethys oceanic domains, respectively (Yin & Harrison, 2000; Shi *et al.* 2008; Gehrels *et al.* 2011). As one of the major components of the Himalayan–Tibetan orogen, the Lhasa terrane is located in the southern part of Tibet where it forms a large crustal segment with a width of 100–300 km and a length of *c.* 2000 km (Fig. 1b). It is composed predominantly of the underlying crystalline basement of Precambrian age, Palaeozoic to Mesozoic marine strata and Mesozoic to Cenozoic arc-type volcanic rocks and intrusions (Yin & Harrison, 2000; Zhu *et al.* 2011*b* , 2013; Zhang & Santosh, 2012). The Lhasa terrane used to be divided into three sub-terranes called the northern, central and southern sub-terranes, separated by the Shiquan River – Nam Tso and the Luobadui–Milashan faults, respectively. Nowadays, with the discovery of eclogite in the Sumdo Complex and blueschist in Pana, ~ 80 km west of Sumdo, a new subdivision scheme has been proposed, suggesting that the Lhasa terrane consists of two discrete crustal fragments, the south and north Lhasa terranes, the latter of which includes the former central

https://doi.org/10.1017/S001675681800033X Published online by Cambridge University Press

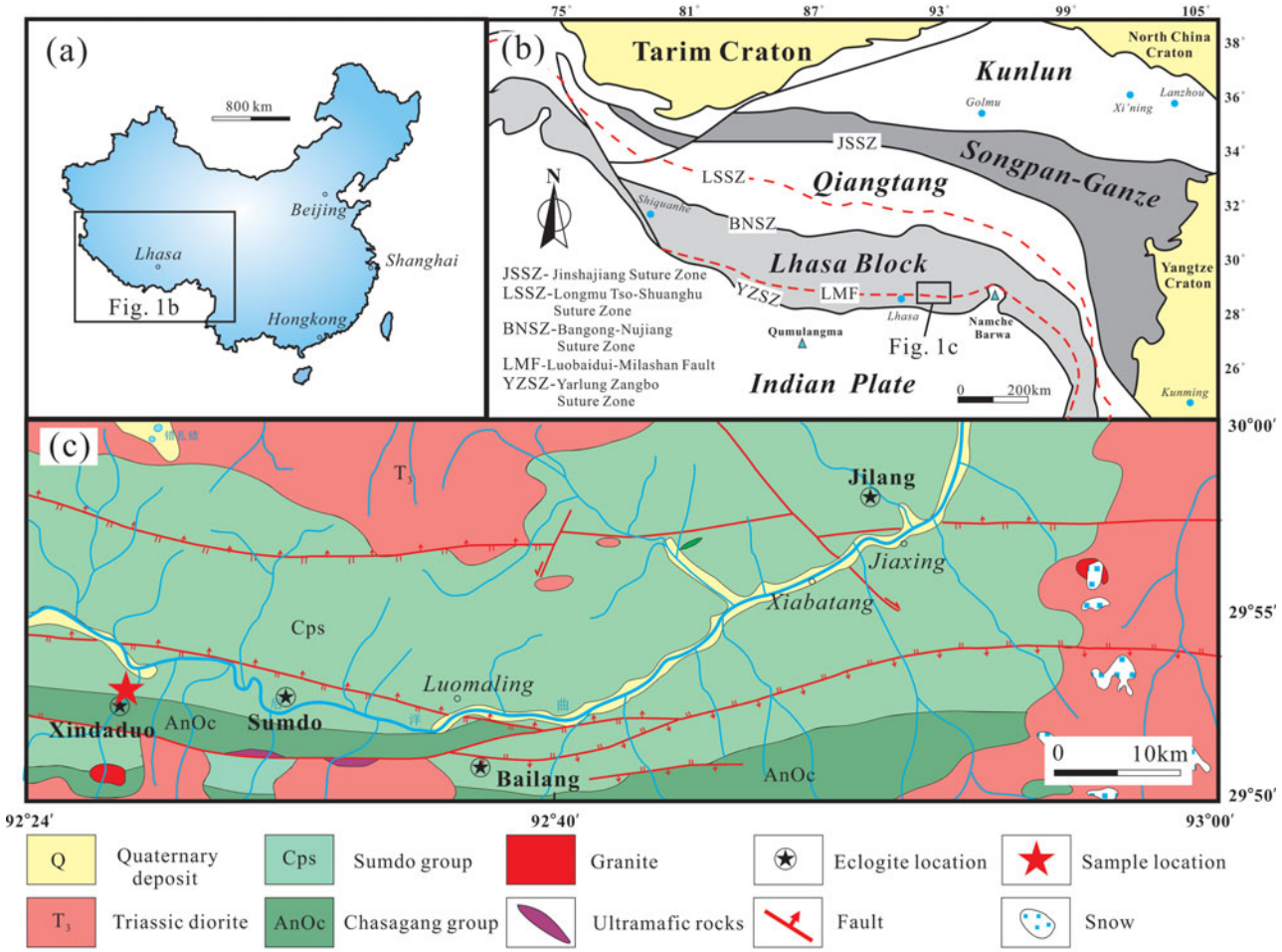

Figure 1. (Colour online) (a) Outline map of China with the location of the Tibetan Plateau. (b) Sketch map of the Tibetan Orogen and its major blocks and suture zones. (c) Simplified geological map of the Sumdo area, showing the four major eclogite occurrences and the sampling location. Modified after Zhang *et al.* (2018).

and northern Lhasa sub-terranes as described above (Liu *et al.* 2009; Yang *et al.* 2009; Xu, Z. *et al.* 2015).

The eclogite-bearing Sumdo Complex in the Lhasa terrane forms an E–W-trending belt at least 100 km long, located *c.* 180 km east of Lhasa City. It consists predominantly of metamorphosed quartzite and pelitic schist, with minor marble, metabasic lenses and serpentinized ultramafic bodies. Eclogite occurs mainly in four locations in the Sumdo Complex, which are the Xindaduo, Sumdo, Bailang and Jilang areas from west to east (Fig. 1c). It can be divided into three types, bimineralic eclogite, phengite eclogite and glaucophane eclogite, by index mineral. The eclogite lenses are hosted by epidote-amphibolite, garnet-bearing mica schist and quartzite, occurring successively as the colour gradually becomes lighter. Fresh eclogites with garnet–omphacite mineral assemblages are preserved only in some of the cores of the metabasic boudins, which otherwise contain amphibolite-facies mineral assemblages in the boudin rims. The investigated garnet-bearing mica schist sample 13SD24 is located in the newly investigated Xindaduo area (29° 51.8′ N, 92° 26.1′ E) in the Sumdo Complex (Fig. 1c), *c.* 500 m from the fresh phengite eclogite bodies and in direct contact with the epidote-amphibolite and quartzite (Fig. 2a, b), the former of which is recognized as the retrograde equivalent of the eclogite.

3. Petrology and mineralogy

The garnet-bearing mica schist is khaki or dark grey in surface colour and well foliated in hand specimen, consisting of garnet (5–10 %), muscovite (15–20 %), albite (10–15 %) and quartz (50–55 %), with minor chlorite, which is partly transformed from biotite, rutile, sphene and apatite. Garnet occurs as euhedral to subhedral porphyroblasts with varying sizes from 0.5 to 2.0 mm, containing inclusions of quartz and phengite in the core–mantle section and quartz, albite, rutile and apatite in the rim. A quartz inclusion with radial fractures was also found in the rim of one garnet porphyroblast (Fig. 2c, d). Some garnet grains are characterized by a subhedral core and surrounded by a newly grown euhedral rim. The rims of the garnet or edges along the cracks have been partly altered by chlorite during retrograde metamorphic stages (Fig. 2e).

Garnet and other rock-forming minerals were analysed by a JEOL JXA-8230 electron microprobe microanalyser (EPM) at the State Key Laboratory

https://doi.org/10.1017/S001675681800033X Published online by Cambridge University Press

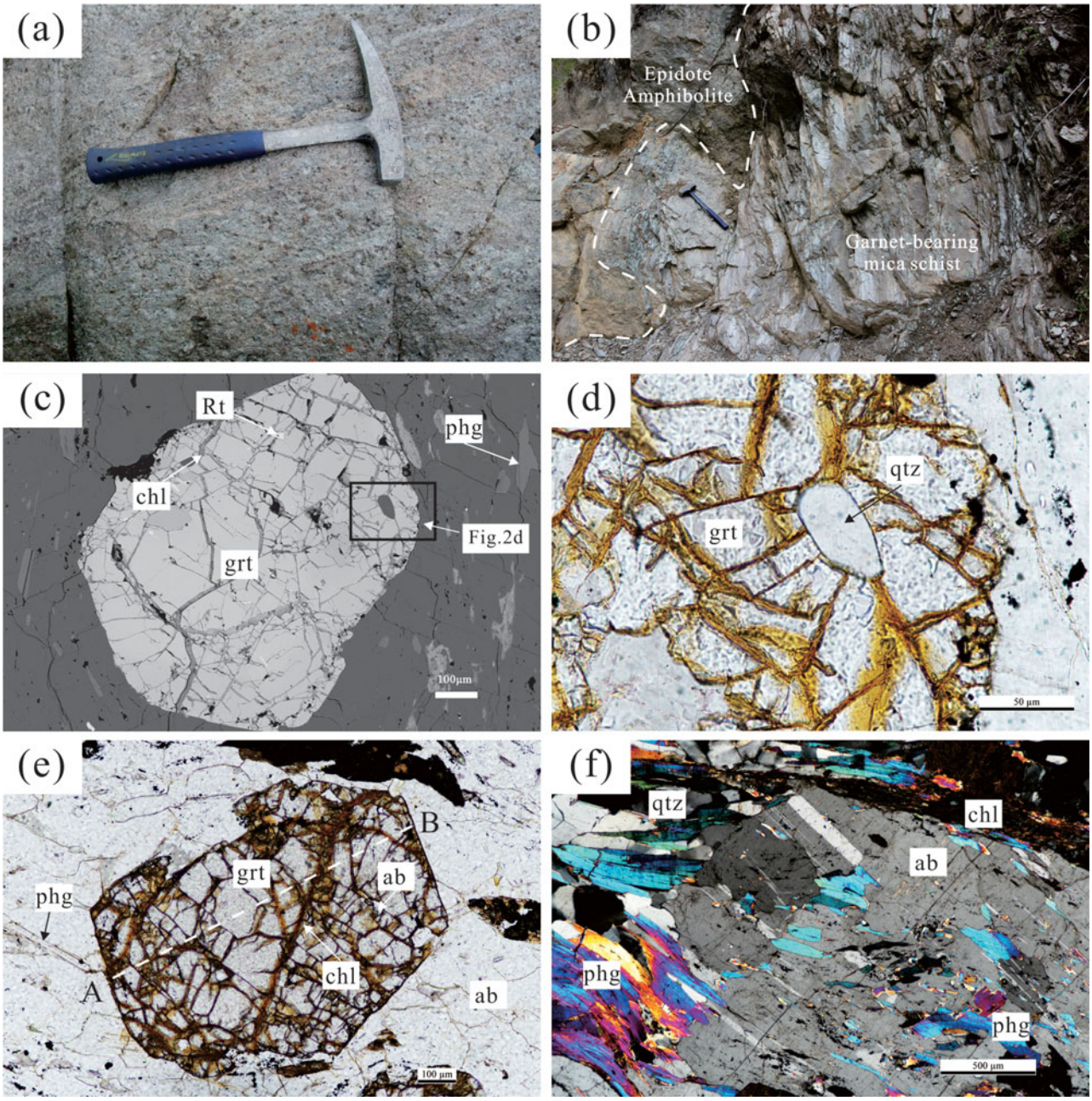

Figure 2. (Colour online) Field occurrences and photomicrographs of the garnet-bearing mica schist 13SD24 from the Xindaduo area, Sumdo Complex. (a) The field occurrence of the garnet-bearing mica schist; hammer for scale is 30 cm long. (b) The relationship of the garnet-bearing mica schist and the epidote-amphibolite. (c) Back-scattered electron (BSE) image showing garnet porphyroblast with inclusions of rutile and quartz surrounded by radial cracks. (d) Quartz inclusion surrounded by chlorite-mineralized radial cracks in garnet; magnification of (c). (e) Garnet porphyroblast with idiomorphic rim, showing different stages of growth. The microprobe analysis profile is shown as line A–B. (f) Albite porphyroblast with muscovite and chlorite inclusions, showing the mineral assemblage in the matrix.

of Marine Geology (Tongji University). Operating conditions were 15 kV acceleration voltage, 10 nA beam current and 0–5 μm beam diameter. Natural and synthetic mineral standards (SPI) were used to calibrate all quantitative analyses and a ZAF correction was used for data reduction. Representative mineral compositions are listed in Table 1. A garnet porphyroblast (0.9 mm in diameter) in garnet-bearing mica schist sample 13SD24 is characterized by an almandine-rich core–mantle section ($Alm_{75–80}Prp_{5–12}Grs_{7–9}Spss_{2–11}$) and a grossular-rich rim ($Alm_{56–68}Prp_{6–11}Grs_{21–29}Spss_{1–9}$). The analytical results from the EPM show that X_{Prp} increases a little bit from the core to the mantle and reaches its peak content (0.12) in the inner rim of the garnet and then decreases towards the outer rim (0.11–0.06). The X_{Spss} profile is characterized by a bell-shaped pattern, which is the opposite trend to X_{Prp}. The X_{Grs} content is constant from the garnet core to the mantle (0.08–0.09) and increases rapidly from the inner rim to the outer rim (0.09–0.29) at the simultaneous expense of X_{Alm} (Figs 2e, 3a; Table 1).

https://doi.org/10.1017/S001675681800033X Published online by Cambridge University Press

Table 1. Representative EPM analysis for the garnet-bearing mica schist from the Xindaduo area of the Sumdo Complex.

Mineral	Grt-c	Grt-c	Grt-m	Grt-m	Grt-r	Grt-r	Phg-g	Phg-m	Ab	Ab	Chl	Chl
SiO_2	36.64	36.93	36.73	36.58	37.32	37.11	51.59	48.97	69.47	68.77	26.48	26.65
TiO_2	0.13	0.02	0.00	0.04	0.02	0.07	0.30	0.45	0.00	0.00	0.16	0.07
Al_2O_3	20.20	19.97	20.16	20.98	20.32	20.27	27.77	30.96	19.11	19.37	18.39	18.39
Cr_2O_3	0.00	0.03	0.00	0.03	0.02	0.02	0.02	0.03	0.03	0.05	0.06	0.02
FeO	33.81	33.83	35.67	36.65	30.91	26.65	2.35	2.18	0.06	0.05	31.86	30.40
MnO	4.45	4.77	0.85	1.42	0.30	3.87	0.06	0.00	0.00	0.00	0.39	0.39
MgO	1.14	1.21	2.57	2.48	2.70	1.36	3.03	2.03	0.00	0.00	10.38	10.94
CaO	2.78	3.09	2.88	2.30	7.65	9.96	0.04	0.02	0.18	0.20	0.06	0.11
Na_2O	0.09	0.13	0.16	0.16	0.08	0.12	0.62	1.01	11.43	11.34	0.13	0.18
K_2O	0.00	0.00	0.02	0.03	0.00	0.02	10.39	10.09	0.04	0.05	0.12	0.08
Totals	99.24	99.98	99.04	100.67	99.32	99.45	96.17	95.74	100.32	99.83	88.03	87.23
O	12.00	12.00	12.00	12.00	12.00	12.00	11.00	11.00	8.00	8.00	14.00	14.00
Si	3.01	3.01	2.99	2.93	2.99	2.98	3.41	3.25	3.02	3.00	2.89	2.91
Ti	0.01	0.00	0.00	0.00	0.00	0.00	0.02	0.02	0.00	0.00	0.01	0.01
Al	1.96	1.92	1.93	1.98	1.92	1.92	2.16	2.42	0.98	1.00	2.36	2.37
Cr	0.00	0.00	0.00	0.00	0.00	0.00	0.00	0.00	0.00	0.00	0.01	0.00
Fe^{3+}	0.03	0.08	0.12	0.17	0.10	0.13	0.00	0.00	0.00	0.00	0.00	0.00
Fe^{2+}	2.29	2.22	2.31	2.29	1.97	1.66	0.13	0.12	0.00	0.00	2.90	2.77
Mn	0.31	0.33	0.06	0.10	0.02	0.26	0.00	0.00	0.00	0.00	0.04	0.04
Mg	0.14	0.15	0.31	0.30	0.32	0.16	0.30	0.20	0.00	0.00	1.69	1.78
Ca	0.25	0.27	0.25	0.20	0.66	0.86	0.00	0.00	0.01	0.01	0.01	0.01
Na	0.01	0.02	0.03	0.03	0.01	0.02	0.08	0.13	0.96	0.96	0.03	0.04
K	0.00	0.00	0.00	0.00	0.00	0.00	0.88	0.86	0.00	0.00	0.02	0.01
X_{Prp}	0.05	0.05	0.11	0.10	0.11	0.06						
X_{Alm}	0.77	0.75	0.79	0.80	0.66	0.56						
X_{Grs}	0.08	0.09	0.09	0.07	0.22	0.29						
X_{Spss}	0.10	0.11	0.02	0.03	0.01	0.09						

Grt-c – garnet core; Grt-m – garnet mantle; Grt-r – garnet rim; Phg-g – phengite in garnet rim; Phg-m – matrix phengite. The mineral formulae were calculated with the program AX2.

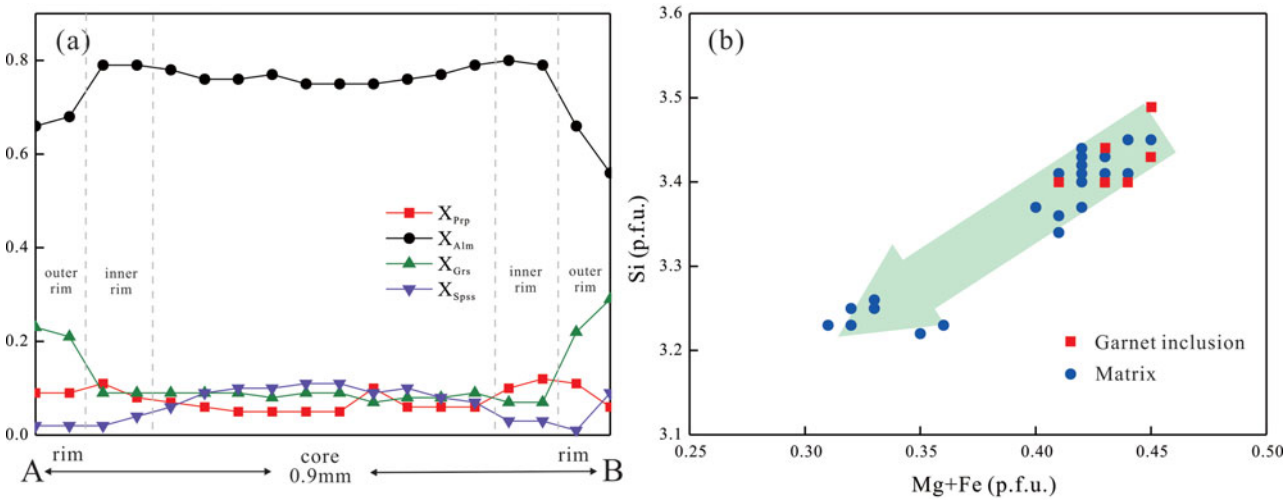

Figure 3. (Colour online) (a) Microprobe analysis profile of the garnet porphyroblast in Figure 2e, showing the variation of four end-members. Prp – pyrope; Alm – almandine; Grs – grossular; Spss – spessartine. (b) The Si v. (Fe + Mg) diagram for phengite from the Xindaduo garnet-bearing mica schist.

Phengite from the garnet-bearing mica schist is included in the garnet or in the matrix and coexists with albite (Fig. 2f). Some of the phengites in the garnets have higher Si (3.4–3.5 p.f.u.) and Mg + Fe contents compared with the ones in the matrix (Fig. 3b), which indicates a higher pressure is preserved in the garnet than in the matrix. Albite is subhedral with a rhombic cross-section and a size of 3–6 mm by 1–3 mm. It commonly contains inclusions of phengite yielding a typical sieve texture (Fig. 2f). Chlorite is mainly preserved in the matrix with quartz and muscovite. Some chlorite occurs within the rims or cracks of the garnet as an alteration product (Fig. 2d, f).

4. Phase equilibrium calculation

The X-ray fluorescence (XRF) analysis was obtained at the China National Research Centre for Geoanalysis. The bulk-rock composition analysed by XRF and the calculated molecular ratios for phase equilibrium modelling of the garnet-bearing mica schist 13SD24 are shown in Table 2. This sample is rich in SiO_2 and Al_2O_3 and depleted in MgO, FeO and CaO, indicating a pelitic rock composition. According to the bulk-rock composition and mineral assemblage, the model system NCKFMASH (Na_2O–CaO–K_2O–FeO–MgO–Al_2O_3–SiO_2–H_2O) was chosen to

https://doi.org/10.1017/S001675681800033X Published online by Cambridge University Press

Table 2. Bulk-rock composition and calculated modal amounts for the garnet-bearing mica schist from the Xindaduo area of the Sumdo Complex.

Oxide	SiO_2	TiO_2	Al_2O_3	Fe_2O_3	FeO	MnO	MgO	CaO	Na_2O	K_2O	LOI		Total
wt %	72.01	0.57	13.00	0.75	2.98	0.07	1.53	0.94	2.15	2.82	2.42		99.24
Cation	**Si**		**Al**	**Fe^{3+}**	**Fe^{2+}**		**Mg**	**Ca**	**Na**	**K**	**O**	**H**	**O**
mol %	70.65		15.03	0.55	2.44		2.24	0.99	4.09	3.53	174.15	40.00	20.00

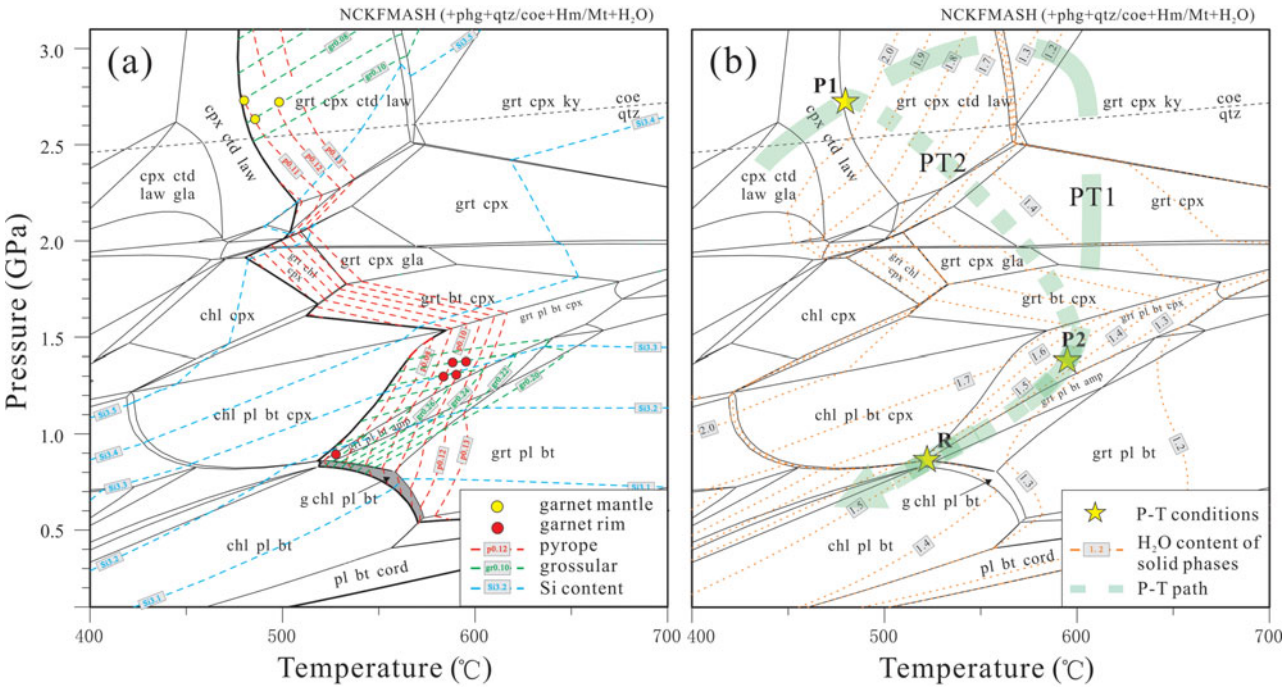

Figure 4. (Colour online) Pseudosection of the garnet-bearing mica schist calculated with Domino/Theriak in the model system NCKFMASH. (a) Pseudosection with isopleths of pyrope (red dashed line) and grossular (green dashed line) in garnet and Si in muscovite (blue dashed line). The garnet mantle and rim compositions are plotted as yellow and red dots, respectively. (b) Pseudosection with isopleths of the H_2O content of all solid phases in the model system and the derived *P–T* path of the garnet-bearing mica schist.

calculate the *P–T* pseudosection. MnO is omitted as it is only preserved in garnet and has little effect on the phase relations according to the database used for the calculation. TiO_2 is also omitted because it is only present in the accessory minerals like rutile and sphene. Quartz/coesite, phengite, iron oxide and H_2O, assumed to be fluid phases, are considered to be in excess. Pseudosections were calculated with Domino/Theriak version 04 02 2017 (De Capitani & Petrakakis, 2010), using the tcdb55c2d database of Holland & Powell (1998). Activity–composition relationships are those presented for garnet (White, Pomroy & Powell, 2005), clinopyroxene (Green, Holland & Powell, 2007), biotite (Powell & Holland, 1999), chlorite (Holland, Baker & Powell, 1998) and phengite (Coggon & Holland, 2002). Isopleths of X_{Prp} and X_{Grs} of garnet and the Si content of phengite contour the pseudosection to obtain the metamorphic conditions of different stages (Fig. 4a). Contours of the H_2O content of solid phases in the system further constrain the metamorphic processes and provide the basis for the discussion on the fluid behaviour during prograde and retrograde metamorphism (Fig. 4b).

The pseudosection is calculated at temperatures from 400 to 700 °C and at less than 3.0 GPa, within a low– medium-temperature metamorphic region. Garnet appears in the area of > *c*. 500 °C and is replaced by chlorite at low pressure, which is concordant with the petrological investigations (Fig. 2c–e). The current stable assemblage of grt + chl + pl + bt (mu + qtz + hm + H_2O) is equilibrated at *c*. 520–570 °C, 0.5–0.9 GPa. As garnet is partially replaced by chlorite at the rim, notably the assemblage should exclude garnet and turn towards a low temperature (Fig. 4a). The isopleths of X_{Prp} and X_{Grs} were contoured to constrain the *P–T* conditions during the growth and regrowth of garnet. The red dashed line in Figure 4a indicates the X_{Prp} isopleths of garnet with a steep slope and increase with temperature, which is suitable as the indicator of temperature. The X_{Grs} isopleths with a green dashed line have a medium positive slope in the high-pressure area of the pseudosection (2.5–3.0 GPa). The ones with high X_{Grs} values (0.2–0.3) were plotted in the medium-pressure field (0.8–1.5 GPa), showing both positive and negative gentle slopes. The variation of X_{Grs} is based on the changes

https://doi.org/10.1017/S001675681800033X Published online by Cambridge University Press

of pressure and is little effected by temperature, making it a good geobarometer for the investigated sample. The Si content isopleths of phengite were also plotted by a blue dashed line to constrain the variations in pressure of the calculated mineral assemblages (Fig. 4a).

The results of the EPM analysis of the garnet, shown by the yellow and red circles, are plotted according to the calculated isopleth values on the pseudosection. The core–mantle section of the garnet porphyroblast (Figs 2e, 3a) was plotted with a yellow circle at 480–500 °C and 2.6–2.7 GPa (stage P1 in Fig. 4b), which is in the LT–HP eclogite-facies metamorphic field. The inner rim with higher X_{Grs} and similar X_{Prp} values, shown by red circles, plots in a narrow *P–T* area of 580–600 °C and pressure of 1.3–1.4 GPa (stage P2 in Fig. 4b). It also seems reasonable to obtain lower *P–T* conditions (*c*. 1 GPa) from this rim composition based on the lower intercept of the X_{Grs} and X_{Prp}. In combination with the Si contents (3.4 p.f.u.) of phengite included in the garnet rim, we deduced that the higher intercept with the higher pressure is more reliable. The temperature recorded by the garnet inner rim is *c*. 100 °C higher than what is recorded by the adjacent garnet mantle. It is not difficult to figure out that the temperature interval is caused by the sudden changes of grossular contents in the garnet porphyroblast. However, what kind of kinetic mechanism caused this situation will be discussed in the following section. The EPM composition on the outer rim of the garnet is plotted at 530 °C, 0.9 GPa (stage R in Fig. 4b), which is similar to the *P–T* conditions constrained by the current mineral assemblage. This amphibolite-facies condition was interpreted to represent the final metamorphic stage recorded by the garnet-bearing mica schist, as the fluid content of the solid phases in the system will be constant along the following retrograde *P–T* path, making it hard for the rock to record the later metamorphic processes (Guiraud, Powell & Rebay, 2001; Wei & Powell, 2004). With the help of the EPM analytical results for the garnet and the calculated isopleths in the pseudosection, three metamorphic stages were recorded by the garnet porphyroblast (Fig. 2e), named as P1, P2 and R, representing the prograde, peak temperature and retrograde stages of the garnet-bearing mica schist in the Xindaduo area of the Sumdo Complex. Two tentative *P–T* paths were proposed to illustrate the metamorphic evolution, named as PT1 and PT2. They share the same trajectory from the peak temperature stage (P2) to the retrograde stage (R) and experienced cooling with decompression processes. However, there are two options for the process from stage P1 to P2. The rock experiences a *P–T* increase to the UHP peak metamorphic stage, followed by an isothermal decompression process along the PT1 path. During the *P–T* increase, the rock experiences a dehydration process with H_2O content in the solid phases decreasing from > 2.0 to 1.2, and then rehydration when the pressure drops down to stage P2. Along the PT2 path, P1 was the peak pressure stage and reached a peak temperature P2 by heating while experiencing decompression. The fluids will also release from the system during this process as in the PT1 situation. It is worth noting that the H_2O content decreased a little bit during retrogression in the *P–T* area of 590–610 °C and 1.4–1.6 GPa in both the PT1 and PT2 paths, which may result in the regrowth of both rock-forming and accessory minerals like zircon, making it possible to relate the metamorphic process to the geochronological data.

5. LA-MC-ICP-MS zircon U–Pb ages

Zircons from the garnet-bearing mica schist sample 13SD24 were selected for isotopic U–Pb dating. Cathodoluminescence (CL) imaging was conducted with a FEI Nova nanoSEM 450 at the Institute of Geology, Chinese Academy of Geological Science. The zircon LA-MC-ICP-MS U–Pb isotopic analysis was performed at the Tianjin Institute of Geology and Mineral Resources on a Neptune mass spectrometer from the Thermo Fisher Company. Detailed instrumental parameters and analytical procedures are those described by Li *et al.* (2010). The age calculation, common Pb correction and concordia plots were made using the program from Andersen (2002) and Isoplot (Ludwig, 2003). Results of the zircon LA-MC-ICP-MS U–Pb dating are given in Table 3.

Zircons from the garnet-bearing mica schist are colourless, stubby, subhedral to euhedral in shape, and oblong to spherical, with lengths of *c*. 80–180 μm. CL images show obvious core–rim structures for some of the zircons, with partly oscillatory zoning or sector patterns of the cores, attributed to their detrital origin (Fig. 5). Zircon rims exhibit blurred patchy zoning or are homogeneous with low luminescence, suggesting recrystallization of detrital zircons or metamorphic growth (Corfu *et al.* 2003; Wu & Zheng, 2004). Forty-five analyses were obtained with ^{206}Pb–^{238}U ages ranging from 228 ± 2 Ma to 1816 ± 19 Ma, with age peaks at 234 Ma, 409 Ma and 575 Ma, etc. from the relative probability diagram (Fig. 6b). Seven analyses from zircon rims appearing dark in CL imaging and with low Th/U ratios (0.01–0.05) yielded a lower intercept age of 229.7 ± 3.5 Ma (MSWD = 1.2) from the Tera-Wasserburg concordia diagram, which is interpreted as dating the metamorphic event in Triassic time (Fig. 6a; Table 3).

6. Discussion

6.a. Metamorphic evolution of the garnet-bearing mica schist in the Xindaduo area

The Sumdo Complex is an E–W-trending, (U)HP metamorphic belt that extends for over 100 km across the middle part of the Lhasa terrane. The discovery of eclogite in several locations along the Sumdo Complex led to a reinterpretation of the tectonic evolution of the Lhasa terrane (Yang *et al.* 2009; Xu, Z. *et al.*

https://doi.org/10.1017/S001675681800033X Published online by Cambridge University Press

Table 3. LA-MC-ICP-MS U–Pb analysis on zircons of the garnet-bearing mica schist from the Xindaduo area of the Sumdo Complex.

Spots	Content ($\times 10^{-6}$)			Isotopic ratios						Age (Ma)					
13SD24	Pb	U	Th/U	$^{206}Pb/^{238}U$	1σ	$^{207}Pb/^{235}U$	1σ	$^{207}Pb/^{206}Pb$	1σ	$^{206}Pb–^{238}U$	1σ	$^{207}Pb–^{235}U$	1σ	$^{207}Pb–^{206}Pb$	1σ
1	99	1105	0.19	0.0928	0.0010	0.7786	0.0107	0.0609	0.0007	572	6	585	8	634	25
2	22	355	0.33	0.0637	0.0009	0.4838	0.0092	0.0550	0.0008	398	6	401	8	414	31
3	90	1288	0.09	0.0704	0.0008	0.7444	0.0114	0.0766	0.0009	439	5	565	9	1112	24
4	38	1117	0.02	0.0368	0.0004	0.2905	0.0041	0.0573	0.0007	233	2	259	4	503	27
5	96	2820	0.03	0.0370	0.0004	0.2685	0.0039	0.0527	0.0007	234	2	241	4	315	28
6	162	714	0.15	0.2292	0.0024	3.4226	0.0470	0.1083	0.0013	1330	14	1510	21	1771	22
7	28	160	0.83	0.1659	0.0017	1.7280	0.0247	0.0755	0.0010	990	10	1019	15	1082	26
8	9	64	0.59	0.1461	0.0015	1.3999	0.0256	0.0695	0.0012	879	9	889	16	914	35
9	29	371	0.14	0.0845	0.0009	0.6649	0.0097	0.0571	0.0007	523	6	518	8	495	28
10	43	157	0.58	0.2591	0.0027	3.6456	0.0513	0.1021	0.0012	1485	15	1560	22	1662	23
11	138	970	0.06	0.1469	0.0016	2.0094	0.0292	0.0992	0.0012	884	10	1119	16	1609	22
12	65	832	0.04	0.0821	0.0009	0.7879	0.0114	0.0696	0.0008	509	5	590	9	916	25
13	13	171	0.72	0.0728	0.0008	0.5886	0.0103	0.0586	0.0009	453	5	470	8	553	35
14	71	2095	0.02	0.0371	0.0004	0.2652	0.0039	0.0519	0.0006	235	3	239	3	282	28
15	76	471	0.63	0.1472	0.0017	1.5236	0.0222	0.0751	0.0009	885	10	940	14	1070	24
16	70	2072	0.01	0.0367	0.0004	0.2696	0.0037	0.0533	0.0006	232	2	242	3	341	27
17	6	74	0.06	0.0890	0.0009	0.7647	0.0181	0.0623	0.0014	549	6	577	14	686	48
18	24	543	0.12	0.0452	0.0005	0.3692	0.0055	0.0593	0.0008	285	3	319	5	578	29
19	27	571	0.17	0.0479	0.0005	0.4576	0.0066	0.0692	0.0009	302	3	383	6	906	27
20	95	270	0.52	0.3254	0.0033	5.1937	0.0707	0.1158	0.0014	1816	19	1852	25	1892	21
21	73	202	0.84	0.3180	0.0033	4.9737	0.0674	0.1134	0.0013	1780	18	1815	25	1855	21
22	80	267	0.90	0.2636	0.0027	3.4517	0.0470	0.0950	0.0011	1508	15	1516	21	1528	22
23	20	208	0.97	0.0830	0.0009	0.6831	0.0118	0.0597	0.0009	514	6	529	9	592	34
24	79	1726	0.13	0.0483	0.0005	0.3620	0.0049	0.0544	0.0007	304	3	314	4	388	27
25	15	225	0.34	0.0661	0.0007	0.5029	0.0086	0.0552	0.0009	412	4	414	7	421	35
26	62	360	0.34	0.1662	0.0017	1.8749	0.0255	0.0818	0.0010	991	10	1072	15	1241	23
27	92	915	0.15	0.0999	0.0011	1.0548	0.0156	0.0766	0.0009	614	7	731	11	1111	24
28	88	332	0.32	0.2510	0.0026	3.9031	0.0529	0.1128	0.0013	1444	15	1614	22	1844	21
29	53	832	0.05	0.0641	0.0007	0.7402	0.0104	0.0838	0.0010	401	4	563	8	1287	24
30	12	105	1.15	0.0937	0.0010	0.6326	0.0141	0.0490	0.0010	577	6	498	11	146	50
31	37	1013	0.05	0.0379	0.0004	0.3071	0.0045	0.0588	0.0008	240	2	272	4	561	29
32	113	1249	0.05	0.0969	0.0011	0.8401	0.0120	0.0629	0.0007	596	6	619	9	703	25
33	9	87	0.77	0.0875	0.0009	0.7578	0.0174	0.0628	0.0014	541	6	573	13	701	46
34	14	277	0.57	0.0451	0.0005	0.3850	0.0072	0.0619	0.0011	284	3	331	6	671	36
35	64	1005	0.24	0.0653	0.0007	0.4911	0.0067	0.0546	0.0007	408	4	406	6	395	27
36	66	190	0.47	0.3227	0.0033	5.0618	0.0685	0.1138	0.0013	1803	18	1830	25	1861	21
37	41	320	0.15	0.1208	0.0018	2.2172	0.0429	0.1331	0.0016	735	11	1186	23	2139	21
38	32	369	0.03	0.0928	0.0010	0.7982	0.0114	0.0624	0.0008	572	6	596	8	688	26
39	19	457	0.04	0.0418	0.0004	0.3923	0.0059	0.0681	0.0009	264	3	336	5	870	29
40	28	76	1.03	0.2998	0.0031	4.3920	0.0611	0.1062	0.0013	1691	17	1711	24	1736	22
41	35	1055	0.02	0.0359	0.0004	0.2565	0.0039	0.0518	0.0007	228	2	232	4	275	31
42	63	241	0.44	0.2421	0.0036	3.2828	0.0596	0.0983	0.0012	1398	21	1477	27	1593	22
43	136	787	0.20	0.1676	0.0019	2.4105	0.0355	0.1043	0.0012	999	11	1246	18	1702	22
44	23	641	0.01	0.0375	0.0004	0.2952	0.0044	0.0571	0.0008	237	2	263	4	495	30
45	12	131	0.73	0.0756	0.0008	0.8321	0.0154	0.0798	0.0014	470	5	615	11	1193	34

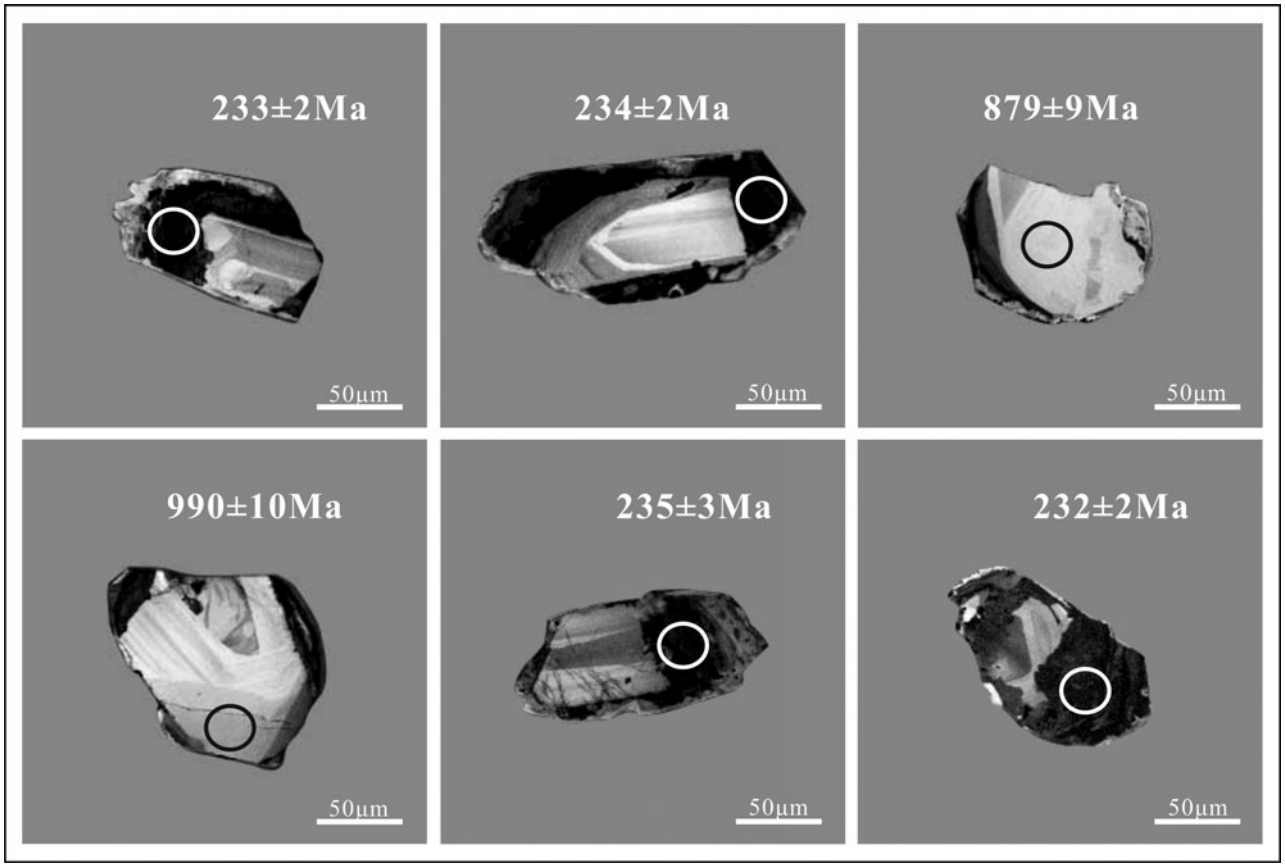

Figure 5. Cathodoluminescence (CL) images of zircons from the garnet-bearing mica schist, showing the positions of the LA-ICP-MS analysis and ages.

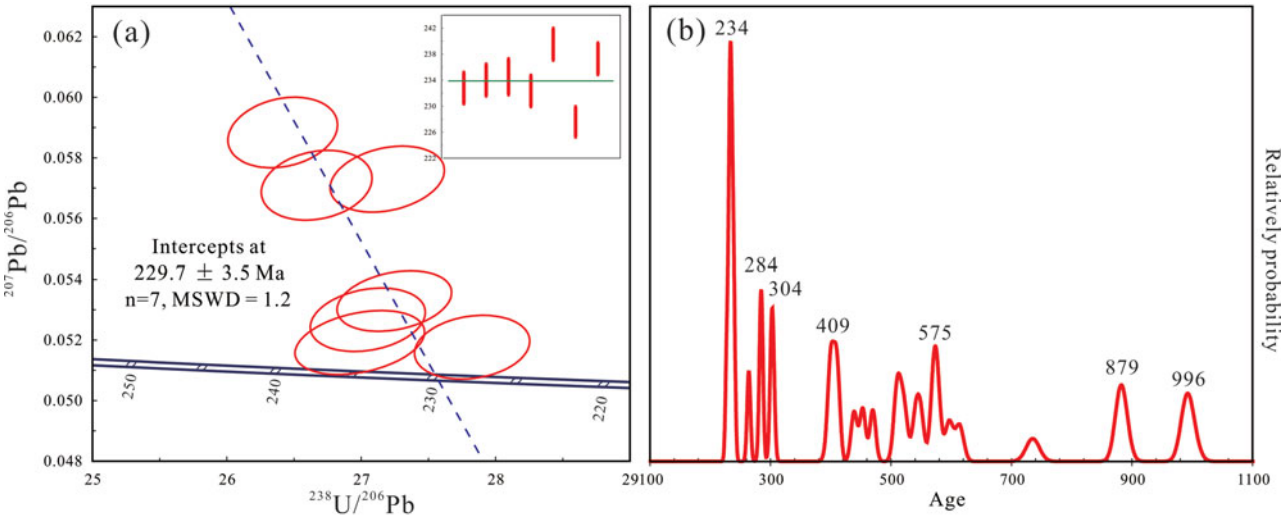

Figure 6. (Colour online) (a) Tera-Wasserburg diagram showing the metamorphic ages of zircons from the garnet-bearing mica schist. The weighted mean age diagram is shown in the upper right corner. (b) Relative probability diagram showing the age peaks of the zircons from the garnet-bearing mica schist from the Xindaduo area.

2015). Two different thermodynamic techniques were applied to different kinds of eclogite in order to calculate the *P–T* path/*P–T* conditions of them and further constrain the physical conditions of the metamorphic processes affecting the Sumdo Complex. With conventional geothermobarometry (Krogh Ravna & Terry, 2004), *P–T* conditions of ∼ 2.7 GPa, 730 °C (Yang *et al.* 2009) and 3.3–3.9 GPa, 760–800 °C (Zhang, Zhang & Zhao, 2011) were calculated for the phengite eclogite in the Sumdo area and 3.4–3.8 GPa, 753–790 °C for the Jilang eclogite (Cheng *et al.* 2012) within the medium-temperature HP and UHP eclogite-facies condition field (Wei, Qian & Tian, 2013). Using the alternative isopleth *P–T* constraint method for phase equilibrium calculations in Thermo-Calc (Powell, Holland & Worley, 1998) and/or Domino/Theriak

https://doi.org/10.1017/S001675681800033X Published online by Cambridge University Press

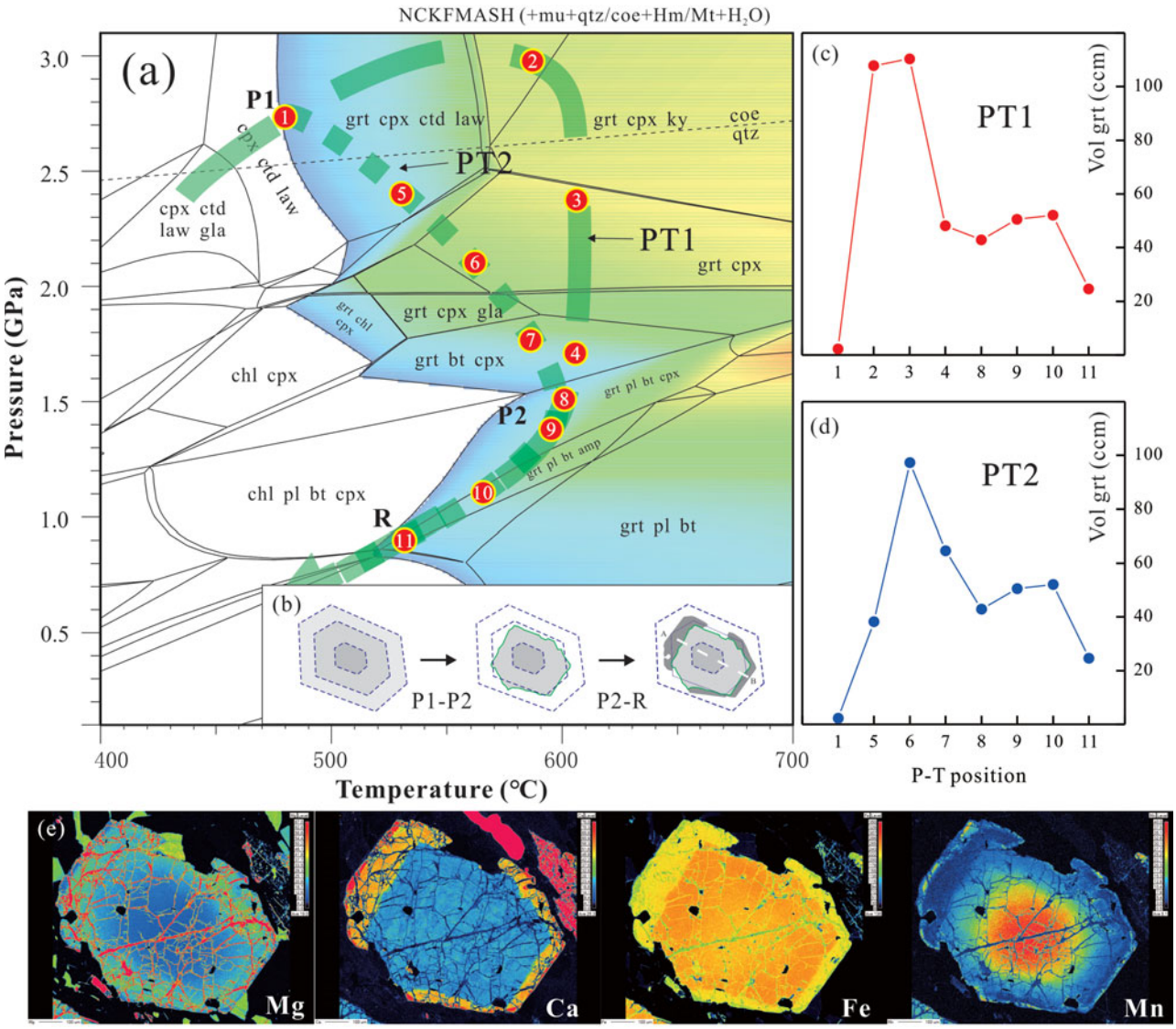

Figure 7. (Colour online) Pseudosection illustrating the metamorphic evolution of garnet from the garnet-bearing mica schist. (a) The rainbow colour shading shows the calculated variation of the garnet volume in the system. The red circles indicate the *P–T* conditions on the *P–T* path. (b) Cartoon showing the metamorphic evolution of the garnet porphyroblast in Figure 2e. (c, d) The calculated volume variation of garnet along the *P–T* paths PT1 and PT2. (e) The wavelength dispersive spectroscopy (WDS) mapping of the garnet porphyroblast showing the regrowth process during retrogression

(De Capitani & Petrakakis, 2010), peak metamorphic *P–T* conditions of *c*. 2.7–3.2 GPa and 610–620 °C were calculated for the phengite and glaucophane eclogites collected in the Sumdo, Xindaduo and Jilang areas, respectively (Fig. 8; Cheng *et al.* 2012; Yang *et al.* 2014; Huang *et al.* 2015; Li *et al.* 2017). The *c*. 100 °C temperature difference between the calculated metamorphic *P–T* conditions obtained by these two methods may be caused either by a different choice of equilibrium minerals or the complicated tectonic evolution of the Sumdo Complex (Zhang *et al.* 2018). Although detailed petrological studies have been performed on eclogite in the Sumdo Complex, less attention has been paid to the metamorphic evolution of its country rock schist. We have chosen a garnet-bearing mica schist in the newly discovered Xindaduo area, which is in the western-most eclogite-bearing area of the Sumdo Complex so far, to perform petrological and geochronological investigations for the first time to clarify the metamorphic *P–T* evolution of this rock and further constrain the metamorphic behaviours of the enclosed eclogite.

Because of the simple mineral assemblage (grt + mu + pl + qtz ± chl ± bt) in the matrix, it is difficult to obtain the *P–T* conditions of the investigated schist with conventional geothermobarometry. The isopleths of X_{Prp} and X_{Grs} of garnet and Si content of phengite were contoured on the pseudosection using the Domino software. The *P–T* conditions for three metamorphic stages are constrained as P1 (480–500 °C, 2.6–2.7 GPa), P2 (580–600 °C, 1.3–1.4 GPa) and R (530 °C, 0.9 GPa), which represent the prograde, temperature peak and retrograde stages. Taking into consideration the H_2O isopleths of the solid phases in the system, two possible *P–T* paths were constructed, which experienced isothermal decompression (PT1) or

https://doi.org/10.1017/S001675681800033X Published online by Cambridge University Press

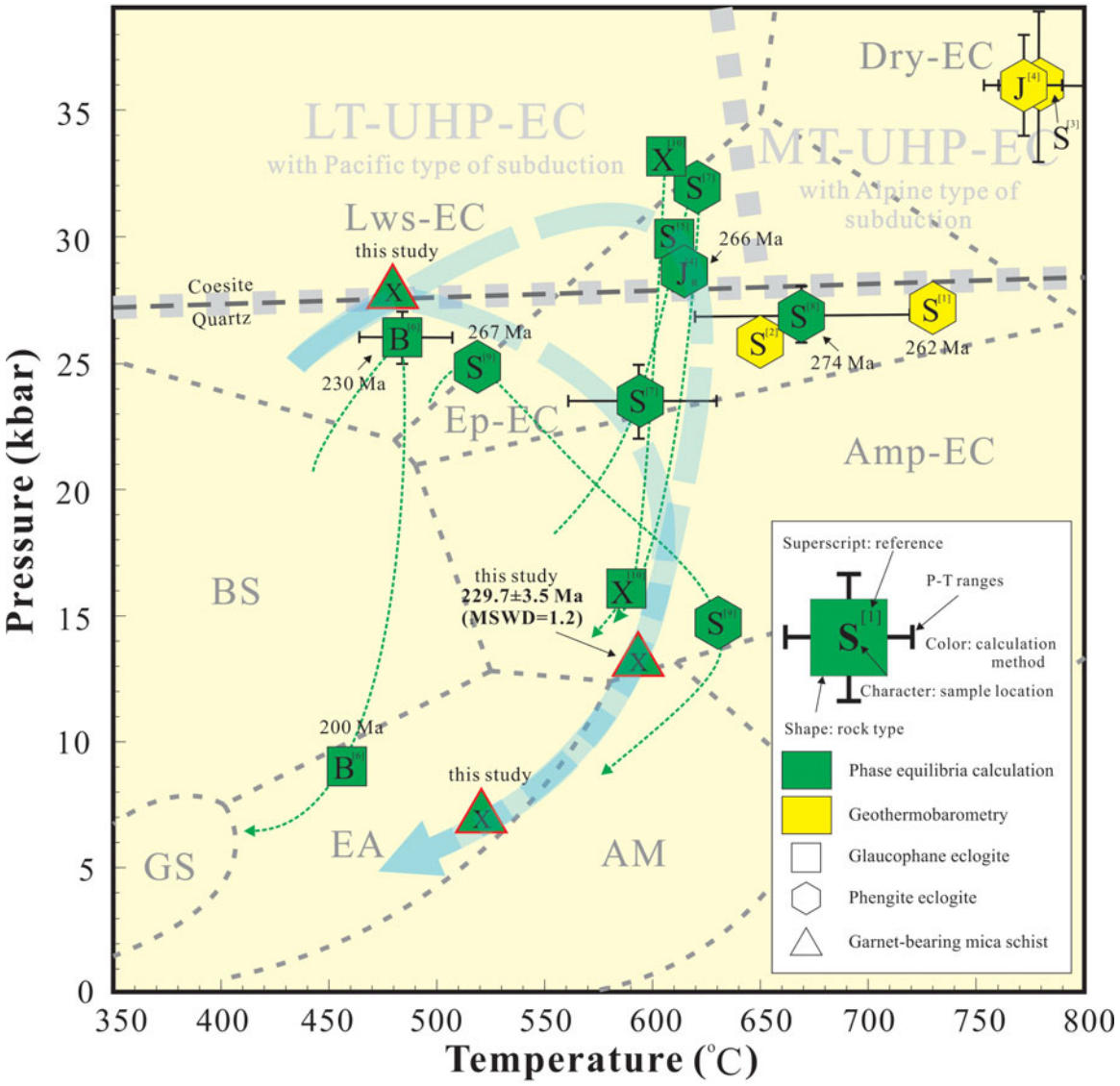

Figure 8. (Colour online) Schematic comparison of *P–T* conditions of metamorphic processes in the eclogites and the investigated garnet-bearing mica schist from the Lhasa terrane, modified after Zhang *et al.* (2018). The *P–T* boundaries of various metamorphic facies are indicated: AM – amphibolite; EA – epidote-amphibolite; GS – greenschist; BS – blueschist schist. The subdivision of eclogite (EC) into amphibole eclogite (Amp-EC), epidote eclogite (Ep-EC), lawsonite eclogite (Lws-EC) and dry eclogite (Dry-EC) is also shown. The discrimination between low-temperature ultrahigh-pressure eclogite (LT-UHP-EC) and medium-temperature ultrahigh-pressure eclogite (MT-UHP-EC) is taken from Wei, Qian & Tian (2013). Characters inside the *P–T* symbols are sample locations: S – Sumdo; J – Jilang; J_R – Jilang recalculated conditions; B – Bailang; X – Xindaduo. References are 1. – Yang *et al.* (2009); 2. – Zeng *et al.* (2009); 3. – Zhang, Zhang & Zhao (2011); 4. – Cheng *et al.* (2012); 5. – Yang *et al.* (2014); 6. – Cheng *et al.* (2015); 7. – Huang *et al.* (2015); 8. – Weller *et al.* (2016); 9. – Cao *et al.* (2017); 10. – Li *et al.* (2017).

heating with a decompression process (PT2). In order to restrict the behaviour of garnet during each possible *P–T* path, 11 *P–T* points were chosen on both paths to calculate the volume variation of the garnet. Points 1, 9 and 11 are equal to the *P–T* conditions of stages P1, P2 and R. The rainbow colour in Figure 7a shows the calculated values of the garnet volume in the system with warmer colours representing higher values. From point 1 to point 4 on the PT1 path, garnet volume increases rapidly during prograde metamorphism and maintains this high volume at the initial stage of the isothermal decompression then decreases to point 4 with a mineral assemblage of grt + bt + cpx (Fig. 7c). Garnet is replaced partly by biotite. The situation is similar to the volume variation trend along PT2, with points 1, 5, 6 and 7 with lower values (Fig. 7d). This process induces garnet growth at pressures higher than 2.0 GPa and consumption when the pressure continuously goes down until the presence of plagioclase in the system, which corresponds to the P1–P2 process in Figure 7b. From point 8 to point 10, both on PT1 and PT2, garnet regrows on the rim with high X_{Grs} and decreases gradually towards point 11, where it is replaced by chlorite. The P2–R process in the cartoon in Figure 7b illustrates the above regrowth process of the high X_{Grs} garnet rim, which explains the sharp and sudden changes in the composition in the garnet rim. The H_2O content in the solid phase between the

https://doi.org/10.1017/S001675681800033X Published online by Cambridge University Press

P–T conditions of points 8–10 also decreases, which can release a certain amount of water into the system not only for garnet growth, but also for the accessory minerals like zircon. With this observation, we infer that the metamorphic zircon rims of the garnet-bearing mica schist grew during *P–T* conditions of *c*. 600 °C, 1.2–1.4 GPa at roughly the peak temperature stage (P2). The absence of the original garnet rim erases the peak pressure and part of the prograde information, making it difficult to discriminate the real *P–T* path from between PT1 and PT2. However, based on the close field relationship between the eclogite and the garnet-bearing mica schist and the *P–T* conditions of the eclogite in the area (Fig. 8), we infer that the PT1 path would be the most reliable scenario for the metamorphic evolution of the schist, which shares the same evolution with the eclogite. The newly reported heating with decompression *P–T* path of the phengite eclogite in the Sumdo area also demonstrates the possibility of a thermal relaxation process during the exhumation of the Sumdo Complex (Cao *et al.* 2017).

6.b. Age constrains and tectonic significance

As one of the Earth's largest active continent–continent collisional orogens, the Tibetan plateau has received plenty of scientific investigations on its magmatism, geophysics, palaeomagnetism and metamorphism (Zhang, J. *et al.* 2012; Klootwijk, 2013; Hébert *et al.* 2014; Zhao *et al.* 2014; Xu, Q. *et al.* 2015; Li *et al.* 2016). The Lhasa terrane in the central part of the Himalayan–Tibetan orogeny plays an important role in understanding the origin and evolution of this giant orogen and also the opening and closure of the Tethys oceans (Zhu *et al.* 2011*a* , 2013; Xu, Z. *et al.* 2015). Metamorphic studies of the Lhasa terrane consider it to have experienced multi-stage and multi-type metamorphism related to subduction and orogeny, including the Neoproterozoic HP to Early Palaeozoic MP metamorphic belt within the north Lhasa terrane, the Late Cretaceous HT/MP to Eocene MP metamorphic belt in the south Lhasa terrane and the Late Permian (U)HP to Triassic MP metamorphic belt represented by the Sumdo Complex (Zhang *et al.* 2014 and references therein). The Sumdo Complex divides the Lhasa terrane into the north Lhasa and south Lhasa terranes based on the existence of eclogite of MORB or OIB affinity, and was thought to form the remnants of the Palaeo-Tethys oceanic floor during Carboniferous time, followed by closure in an intra-oceanic supra-subduction zone environment, finally resulting in the accretion of the Lhasa terrane (Chen *et al.* 2007; Yang *et al.* 2009; Cheng *et al.* 2012, 2015; Zhang *et al.* 2018).

SHRIMP and LA-ICP-MS U–Pb zircon dating as well as whole-rock mineral Sm–Nd and Lu–Hf isotopic dating methods have been performed on the eclogite and yielded 260–274 Ma eclogite-facies metamorphic ages in the Sumdo and Jilang areas (Yang *et al.* 2009; Cheng *et al.* 2012; Weller *et al.* 2016; Cao *et al.* 2017) and an age of *c*. 230 Ma in the Bailang area for the Sumdo Complex, respectively (Cheng *et al.* 2015). No metamorphic ages were obtained from the country rocks of the eclogite until now because of the sedimentary origin of the zircons. Only an ^{40}Ar–^{39}Ar age of 220–230 Ma was obtained from the muscovite of the greenschists from the ductile shear zones in the Sumdo Complex (Li *et al.* 2009). The zircons from the garnet-bearing mica schist in the Xindaduo area were dated by the LA-MC-ICP-MS method. Except for the detrital age peaks shown in the relative probability diagram, seven analytical spots on the high U, low Th/U ratio zircon rims yield a 229.7 ± 3.5 Ma metamorphic age. Based on the fluid content variation and garnet growth phenomenon of the garnet-bearing mica schist, this Triassic age was interpreted to date the amphibolite-facies metamorphism at *c*. 600 °C, 1.2–1.4 GPa during the closure of the Palaeo-Tethys Ocean, which is also concordant with the metamorphic ages from the eclogite. Combined with the close relationship between the eclogite and garnet-bearing mica schist, and their similar *P–T–t* paths, it is reasonable to consider an *in situ* tectonic evolution for them both rather than their being juxtaposed during exhumation. With the 225–210 Ma medium-pressure metamorphism and simultaneous granitic magmatism of post-collisional pluton affinity in the same belt between the south and north Lhasa terranes (Zhang *et al.* 2007, 2014; Dong *et al.* 2011), the Sumdo Complex is supposed to represent a Pacific-type subduction zone, resulting in the collision between the north and south Lhasa terranes.

7. Conclusion

In combination with petrological investigations and pseudosection modelling in the model system NCKFMASH, three metamorphic stages and two possible *P–T* paths are constrained for the garnet-bearing mica schist. P1 (480–500 °C, 2.6–2.7 GPa), P2 (580–600 °C, 1.3–1.4 GPa) and R (530 °C, 0.9 GPa) represent the prograde, temperature peak and retrograde stages, while either isothermal decompression (PT1) or heating with a decompression process (PT2) during retrograde metamorphism is the case for the metamorphic evolution of the garnet-bearing mica schist. The LA-MC-ICP-MS metamorphic U–Pb age of 229.7 ± 3.5 Ma (MSWD = 1.2) was obtained from the zircon rims from the garnet-bearing mica schist, which is interpreted to date the amphibolite-facies metamorphism at *c*. 600 °C, 1.2–1.4 GPa during the closure of the Palaeo-Tethys Ocean, resulting from the collision between the north and south Lhasa terranes.

Acknowledgements. This research is financially supported by the National Science Foundation of China (Nos. 41572051, 41630207, 41572044, 41502039), the Research Founding from the Chinese Academy of Geological Sciences (No. YYWF201702) and the Basic Geological Survey Program of China (No. DD20160022-01). Dr. Chad Deering as

https://doi.org/10.1017/S001675681800033X Published online by Cambridge University Press

the editor and two anonymous reviewers are thanked for their constructive comments that considerately improved the early version of this manuscript.

References

Andersen, T. 2002. Correction of common lead in U–Pb analyses that do not report ^{204}Pb. *Chemical Geology* **192**, 59–79.

Cao, D., Cheng, H., Zhang, L. M. & Wang, K. 2017. Post-peak metamorphic evolution of the Sumdo eclogite from the Lhasa terrane of southeast Tibet. *Journal of Asian Earth Sciences* **143**, 156–70.

Carswell, D. A. 1990. *Eclogite Facies Rocks*. New York: Blackie.

Carswell, D. A. & Cuthbert, S. J. 2003. Ultrahigh pressure metamorphism in the Western Gneiss Region of Norway. In *EMU Notes in Mineralogy, Vol.* **5** (eds D. A. Carswell & R. Compagnoni), pp. 51–73. Budapest: Eötvös University Press.

Chen, S. Y., Yang, J. S., Luo, L. Q., Li, Z. L., Xu, X. Z., Li, T. F., Ren, Y. F. & Li, H. Q. 2007. MORB-type eclogites in the Lhasa block, Tibet, China: petrochemical evidence. *Geological Bulletin of China* **26**, 1327–39 (in Chinese with English abstract).

Cheng, H., Liu, Y., Vervoort, J. D. & Lu, H. 2015. Combined U–Pb, Lu–Hf, Sm–Nd and Ar–Ar multichronometric dating on the Bailang eclogite constrains the closure timing of the Paleo-Tethys Ocean in the Lhasa terrane, Tibet. *Gondwana Research* **28**, 1482–99.

Cheng, H., Zhang, C., Vervoort, J. D., Lu, H., Wang, C. & Cao, D. 2012. Zircon U–Pb and garnet Lu–Hf geochronology of eclogites from the Lhasa Block, Tibet. *Lithos* **155**, 341–59.

Chopin, C. 1984. Coesite and pure pyrope in high-grade blueschists of the Western Alps – a 1st record and some consequences. *Contributions to Mineralogy and Petrology* **86**, 107–18.

Chopin, C. 2003. Ultrahigh-pressure metamorphism: tracing continental crust into the mantle. *Earth and Planetary Science Letters* **212**, 1–14.

Coggon, R. & Holland, T. J. B. 2002. Mixing properties of phengitic micas and revised garnet-phengite thermobarometers. *Journal of Metamorphic Geology* **20**, 683–96.

Coleman, R. G. & Wang, X. 1995. *Ultrahigh-Pressure Metamorphism*. New York: Cambridge University Press.

Corfu, F., Hanchar, J. M., Hoskin, P. W. O. & Kinny, P. 2003. Atlas of zircon textures. *Reviews in Mineralogy and Geochemistry* **53**, 469–500.

De Capitani, C. & Petrakakis, K. 2010. The computation of equilibrium assemblage diagrams with Theriak/Domino software. *American Mineralogist* **95**, 1006–16.

Dong, X., Zhang, Z., Liu, F., Wang, W., Yu, F. & Shen, K. 2011. Zircon U–Pb geochronology of the Nyainqentanglha Group from the Lhasa terrane: new constraints on the Triassic orogeny of the south Tibet. *Journal of Asian Earth Sciences* **42**, 732–9.

Du, J., Zhang, L., Lü, Z. & Chu, X. 2011. Lawsonite-bearing chloritoid–glaucophane schist from SW Tianshan, China: phase equilibria and P–T path. *Journal of Asian Earth Sciences* **42**, 684–93.

Ernst, W. G. 2001. Subduction, ultrahigh-pressure metamorphism, and regurgitation of buoyant crustal slices – implications for arcs and continental growth. *Physics of the Earth and Planetary Interiors* **127**, 253–75.

Ernst, W. G., Hacker, B. R. & Liou, J. G. 2007. Petrotectonics of ultrahigh-pressure crustal and upper-mantle rocks – implications for Phanerozoic collisional orogens. In *Whence the Mountains? Inquiries into the Evolution of Orogenic Systems: A Volume in Honor of Raymond A. Price* (eds J. W. Sears, T. A. Harms & C. A Evenchick), pp. 27–49. Geological Society of America Special Paper no. 433.

Ernst, W. G. & Liou, J. G. 1995. Contrasting plate-tectonic styles of the Qinling-Dabie-Sulu and Franciscan Metamorphic Belts. *Geology* **23**, 353–6.

Ernst, W. G. & Liou, J. G. 2008. High- and ultrahigh-pressure metamorphism – past results, future prospects. *American Mineralogist* **93**, 1771–86.

Gehrels, G., Kapp, P., DeCelles, P., Pullen, A., Blakey, R., Weislogel, A., Ding, L., Guynn, J., Martin, A., McQuarrie, N. & Yin, A. 2011. Detrital zircon geochronology of pre-Tertiary strata in the Tibetan-Himalayan orogen. *Tectonics* **30**, TC5016. doi: 10.1029/2011TC002868.

Green, E., Holland, T. & Powell, R. 2007. An order–disorder model for omphacitic pyroxenes in the system jadeite–diopside–hedenbergite–acmite, with applications to eclogitic rocks. *American Mineralogist* **92**, 1181–9.

Guiraud, M., Powell, R. & Rebay, G. 2001. H_2O in metamorphism and unexpected behaviour in the preservation of metamorphic mineral assemblages. *Journal of Metamorphic Geology* **19**, 445–54.

Hébert, R., Guilmette, C., Dostal, J., Bezard, R., Lesage, G., Bédard, É. & Wang, C. 2014. Miocene post-collisional shoshonites and their crustal xenoliths, Yarlung Zangbo Suture Zone southern Tibet: geodynamic implications. *Gondwana Research* **25**, 1263–71.

Holland, T., Baker, J. & Powell, R. 1998. Mixing properties and activity-composition relationships of chlorites in the system MgO–FeO–Al_2O_3–SiO_2–H_2O. *European Journal of Mineralogy* **10**, 395–406.

Holland, T. J. B. & Powell, R. 1998. An internally consistent thermodynamic data set for phases of petrological interest. *Journal of Metamorphic Geology* **16**, 309–43.

Huang, J., Tian, Z. L., Zhang, C., Yang, J. S. & Chen, M. 2015. Metamorphic evolution of Sumdo eclogite in Lhasa Block of the Tibetan Plateau: phase equilibrium in NCKMnFMASHTO system. *Geology in China* **42**, 1559–71 (in Chinese with English abstract).

Klootwijk, C. 2013. Middle–Late Paleozoic Australia–Asia convergence and tectonic extrusion of Australia. *Gondwana Research* **24**, 5–54.

Krogh Ravna, E. & Terry, M. P. 2004. Geothermobarometry of UHP and HP eclogites and schists – an evaluation of equilibria among garnet–clinopyroxene–kyanite–phengite–coesite/quartz. *Journal of Metamorphic Geology* **22**, 579–92.

Le Goff, E. & Bellevre, M. 1990. Geothermobarometry in albite-garnet orthogneisses: a case study from the Gran Paradiso nappe (Western Alps). *Lithos* **25**, 261–80.

Li, Z. Y., Ding, L., Lippert, P. C., Song, P. P., Yue, Y. H. & van Hinsbergen, D. J. J. 2016. Paleomagnetic constraints on the Mesozoic drift of the Lhasa terrane (Tibet) from Gondwana to Eurasia. *Geology* **44**, 727–30.

Li, H. Q., Xu, Z. Q., Yang, J. S., Cai, Z. H., Chen, S. Y. & Tang, Z. M. 2009. Records of Indosinian orogenesis in Lhasa terrane, Tibet. *Journal of Earth Science* **20**, 348–63.

Li, P., Zhang, C., Liu, X. Y., Shen, T. T., Qiu, T. & Yang, J. S. 2017. The metamorphic processes of the Xindaduo

eclogite in Tibet and its constrain on the evolutionary of the Paleo-Tethys subduction zone. *Acta Petrologica Sinica* **33**, 3753–65 (in Chinese with English abstract).

Li, H. K., Zhu, S. X., Xiang, Z. Q., Su, W. B., Lu, S. N., Zhou, H. Y., Geng, J. Z., Li, S. & Yang, F. J. 2010. Zircon U–Pb dating on tuff bed from Gaoyuzhuang Formation in Yanqing, Beijing: further constraints on the new subdivision of the Mesoproterozoic stratigraphy in the northern North China Craton. *Acta Petrologica Sinica* **26**, 2131–40 (in Chinese with English abstract).

Liou, J. G., Ernst, W. G., Zhang, R. Y., Tsujimori, T. & Jahn, B. M. 2009. Ultrahigh-pressure minerals and metamorphic terranes – the view from China. *Journal of Asian Earth Sciences* **35**, 199–231.

Liou, J. G., Tsujimori, T., Zhang, R. Y., Katayama, I. & Maruyama, S. 2004. Global UHP metamorphism and continental subduction/collision: the Himalayan model. *International Geology Review* **46**, 1–27.

Liu, Y., Liu, H., Theye, T. & Massonne, H.-J. 2009. Evidence for oceanic subduction at the NE Gondwana margin during Permo-Triassic times. *Terra Nova* **21**, 195–202.

Ludwig, K. R. 2003. *User's Manual for Isoplot Version 3.00. A Geochronological Toolkit for Microsoft Excel*. Berkeley Geochronology Center Special Publication no. 4.

Maruyama, S., Liou, J. G. & Terabayashi, M. 1996. Blueschists and eclogites of the world and their exhumation. *International Geology Review* **38**, 485–594.

Menold, C. A., Manning, C. E., Yin, A., Tropper, P., Chen, X. H. & Wang, X. F. 2009. Metamorphic evolution, mineral chemistry and thermobarometry of orthogneiss hosting ultrahigh-pressure eclogites in the North Qaidam metamorphic belt, Western China. *Journal of Asian Earth Sciences* **35**, 273–84.

Pan, G. T., Mo, X. X., Hou, Z. Q., Zhu, D. C., Wang, L. Q., Li, G. M., Zhao, Z. D., Geng, Q. R. & Liao, Z. L. 2006. Spatial-temporal framework of the Gongdese Orogenic Belt and its evolution. *Acta Petrologica Sinica* **22**, 521–33 (in Chinese with English abstract).

Philippot, P. & van Roermund, H. L. M. 1992. Deformation processes in eclogitic rocks – evidence for the rheological delamination of the oceanic-crust in deeper levels of subduction zones. *Journal of Structural Geology* **14**, 1059–77.

Powell, R. & Holland, T. 1999. Relating formulations of the thermodynamics of mineral solid solutions; activity modeling of pyroxenes, amphiboles, and micas. *American Mineralogist* **84**, 1–14.

Powell, R., Holland, T. & Worley, B. 1998. Calculating phase diagrams involving solid solutions via non-linear equations, with examples using THERMOCALC. *Journal of Metamorphic Geology* **16**, 577–88.

Proyer, A. 2003. The preservation of high-pressure rocks during exhumation: metagranites and metapelites. *Lithos* **70**, 183–94.

Shi, R., Yang, J., Xu, Z. & Qi, X. 2008. The Bangong Lake ophiolite (NW Tibet) and its bearing on the tectonic evolution of the Bangong–Nujiang suture zone. *Journal of Asian Earth Sciences* **32**, 438–57.

Smith, D. C. 1988. *Eclogites and Eclogite Facies Rocks*. Amsterdam: Elsevier.

Song, S., Niu, Y., Su, L., Zhang, C. & Zhang, L. 2014. Continental orogenesis from ocean subduction, continent collision/subduction, to orogen collapse, and orogen recycling: the example of the North Qaidam UHPM belt, NW China. *Earth-Science Reviews* **129**, 59–84.

Song, S. G., Zhang, L. F., Niu, Y. L., Su, L., Song, B. & Liu, D. Y. 2006. Evolution from oceanic subduction to continental collision: a case study from the Northern Tibetan Plateau based on geochemical and geochronological data. *Journal of Petrology* **47**, 435–55.

Wei, C. J. 2012. Advance of metamorphic petrology during the first decade of the 21st century. *Bulletin of Mineralogy, Petrology and Geochemistry* **31**, 416–27 (in Chinese with English abstract).

Wei, C. J. & Powell, R. 2004. Calculated phase relations in high-pressure metapelites in the system NKFMASH (Na_2O–K_2O–FeO–MgO–Al_2O_3–SiO_2–H_2O) with application to natural rocks. *Journal of Petrology* **45**, 183–202.

Wei, C. J., Qian, J. H. & Tian, Z. L. 2013. Metamorphic evolution of medium-temperature ultra-high pressure (MT-UHP) eclogites from the South Dabie orogen, Central China: an insight from phase equilibria modelling. *Journal of Metamorphic Geology* **31**, 755–74.

Wei, C. J., Su, X. L., Lou, Y. X. & Li, Y. J. 2009. A new interpretation of the conventional thermobarometry in eclogite: evidence from the calculated PT pseudosections. *Acta Petrologica Sinica* **25**, 2078–88 (in Chinese with English abstract).

Weller, O. M., St-Onge, M. R., Rayner, N., Waters, D. J., Searle, M. P. & Palin, R. M. 2016. U–Pb zircon geochronology and phase equilibria modelling of a mafic eclogite from the Sumdo complex of southeast Tibet: insights into prograde zircon growth and the assembly of the Tibetan plateau. *Lithos* **262**, 729–41.

White, R. W., Pomroy, N. E. & Powell, R. 2005. An in situ metatexite–diatexite transition in upper amphibolite facies rocks from Broken Hill, Australia. *Journal of Metamorphic Geology* **23**, 579–602.

Wu, Y. B. & Zheng, Y. F. 2004. Genetic mineralogy of zircon and its constraints on the interpretation of U–Pb age. *Chinese Science Bulletin* **49**, 1589–604 (in Chinese with English abstract).

Xu, Z., Dilek, Y., Cao, H., Yang, J., Robinson, P., Ma, C., Li, H., Jolivet, M., Roger, F. & Chen, X. 2015. Paleo-Tethyan evolution of Tibet as recorded in the East Cimmerides and West Cathaysides. *Journal of Asian Earth Sciences* **105**, 320–37.

Xu, Q., Zhao, J., Yuan, X., Liu, H. & Pei, S. 2015. Mapping crustal structure beneath southern Tibet: seismic evidence for continental crustal underthrusting. *Gondwana Research* **27**, 1487–93.

Yang, D. M., He, Z. H., Huang, Y. C., Zhao, L. & Dai, L. N. 2005. Metamorphism characteristics of Songduo Group in Menba Township Mozhugongka Country, Tibet and the discussion on its age. *Journal of Jilin University (Earth Science Edition)* **35**, 430–5 (in Chinese with English abstract).

Yang, J. S., Xu, Z. Q., Geng, Q. R., Li, Z. L., Xu, X. Z., Li, T. F., Ren, Y. F., Li, H. Q., Cai, Z. H., Liang, F. H. & Chen, S. Y. 2006. A possible new HP/UHP(?) metamorphic belt in China: discovery of eclogite in the Lhasa Terrane, Tibet. *Acta Geologica Sinica* **80**, 1787–92 (in Chinese with English abstract).

Yang, J. S., Xu, Z. Q., Li, Z. L., Xu, X. Z., Li, T. F., Ren, Y. F., Li, H. Q., Chen, S. Y. & Robinson, P. T. 2009. Discovery of an eclogite belt in the Lhasa block, Tibet: a new border for Paleo-Tethys? *Journal of Asian Earth Sciences* **34**, 76–89.

Yang, X. L., Zhang, L. F., Zhao, Z. D. & Zhu, D. C. 2014. Metamorphic evolution of glaucophane eclogite from Sumdo, Lhasa block of Tibetan Plateau: phase

https://doi.org/10.1017/S001675681800033X Published online by Cambridge University Press

equilibria and metamorphic P–T path. *Acta Petrologica Sinica* **30**, 1505–19 (in Chinese with English abstract).

Yin, A. & Harrison, T. M. 2000. Geological evolution of the Himalayan-Tibet orogen. *Annual Review of Earth and Planetary Sciences* **28**, 211–80.

Zeng, L. S., Liu, J., Gao, L. E., Chen, F. Y. & Xie, K. J. 2009. Early Mesozoic high-pressure metamorphism within the Lhasa Block, Tibet and its implications for regional tectonics. *Earth Science Frontiers* **16**, 140–51 (in Chinese with English abstract).

Zhang, C., Bader, T., van Roermund, H. L. M., Yang, J. S., Shen, T. T., Qiu, T. & Li, P. 2018. The metamorphic evolution and tectonic significance of the Sumdo HP–UHP metamorphic terrane, central-south Lhasa Block, Tibet. In *HP–UHP Metamorphism and Tectonic Evolution of Orogenic Belts* (eds L. Zhang, Z. Zhang, H.-P. Schertl & C. Wei), Geological Society of London, Special Publication no. 474, published online 22 March 2018. doi: 10.1144/SP474.4.

Zhang, C., Bader, T., Zhang, L. & van Roermund, H. 2017. The multi-stage tectonic evolution of the Xitieshan terrane, North Qaidam orogen, western China: from Grenville-age orogeny to early-Paleozoic ultrahigh-pressure metamorphism. *Gondwana Research* **41**, 290–300.

Zhang, Z. M., Dong, X., Santosh, M. & Zhao, G. C. 2014. Metamorphism and tectonic evolution of the Lhasa terrane, Central Tibet. *Gondwana Research* **25**, 170–89.

Zhang, L. F., Ellis, D. J., Arculus, R. J., Jiang, W. & Wei, C. 2003. 'Forbidden zone' subduction of sediments to 150 km depth – the reaction of dolomite to magnesite plus aragonite in the UHPM metapelites from western Tianshan, China. *Journal of Metamorphic Geology* **21**, 523–9.

Zhang, R. Y., Jahn, B. M., Liou, J. G., Yang, J. S., Chiu, H. Y., Chung, S. L., Li, T. F. & Lo, C. H. 2010. Origin and tectonic implication of an UHP metamorphic mafic–ultramafic complex from the Sulu UHP terrane, eastern China: evidence from petrological and geochemical studies of CCSD-Main Hole core samples. *Chemical Geology* **276**, 69–87.

Zhang, J. X., Mattinson, C. G., Meng, F. C., Wan, Y. S. & Tung, K. 2008. Polyphase tectonothermal history recorded in granulitized gneisses from the north Qaidam HP/UHP metamorphic terrane, western China: evidence from zircon U–Pb geochronology. *Geological Society of America Bulletin* **120**, 732–49.

Zhang, Z. M. & Santosh, M. 2012. Tectonic evolution of Tibet and surrounding regions. *Gondwana Research* **21**, 1–3.

Zhang, J., Santosh, M., Wang, X., Guo, L., Yang, X. & Zhang, B. 2012. Tectonics of the northern Himalaya since the India–Asia collision. *Gondwana Research* **21**, 939–60.

Zhang, C., van Roermund, H., Zhang, L. F. & Spiers, C. 2012. A polyphase metamorphic evolution for the Xitieshan paragneiss of the north Qaidam UHP metamorphic belt, western China: in-situ EMP monazite- and U–Pb zircon SHRIMP dating. *Lithos* **136–139**, 27–45.

Zhang, H. F., Xu, W. C., Guo, J. Q., Zong, K. Q., Cai, H. M. & Yuan, H. L. 2007. Indosinian orogenesis of the Gangdise terrane: evidences from zircon U–Pb dating and petrogenesis of granitoids. *Earth Science* **32**, 155–66 (in Chinese with English abstract).

Zhang, D. D., Zhang, L. F. & Zhao, Z. D. 2011. A study of metamorphism of Sumdo eclogite in Tibet, China. *Earth Science Frontiers* **18**, 116–26 (in Chinese with English abstract).

Zhao, J., Zhao, D., Zhang, H., Liu, H., Huang, Y., Cheng, H. & Wang, W. 2014. P-wave tomography and dynamics of the crust and upper mantle beneath western Tibet. *Gondwana Research* **25**, 1690–9.

Zheng, Y. F. 2012. Metamorphic chemical geodynamics in continental subduction zones. *Chemical Geology* **328**, 5–48.

Zheng, Y. F., Fu, B., Gong, B. & Li, L. 2003. Stable isotope geochemistry of ultrahigh pressure metamorphic rocks from the Dabie-Sulu orogen in China: implications for geodynamics and fluid regime. *Earth-Science Reviews* **62**, 105–61.

Zhu, D. C., Zhao, Z. D., Niu, Y. L., Dilek, Y., Hou, Z. Q. & Mo, X. X. 2013. The origin and pre-Cenozoic evolution of the Tibetan Plateau. *Gondwana Research* **23**, 1429–54.

Zhu, D. C., Zhao, Z. D., Niu, Y. L., Dilek, Y. & Mo, X. X. 2011a. Lhasa terrane in southern Tibet came from Australia. *Geology* **39**, 727–30.

Zhu, D.-C., Zhao, Z.-D., Niu, Y., Mo, X.-X., Chung, S.-L., Hou, Z.-Q., Wang, L.-Q. & Wu, F.-Y. 2011b. The Lhasa Terrane: record of a microcontinent and its histories of drift and growth. *Earth and Planetary Science Letters* **301**, 241–55.

https://doi.org/10.1017/S001675681800033X Published online by Cambridge University Press